The mean shape of transition and first-passage paths

Won Kyu Kim and Roland R. Netz

Citation: The Journal of Chemical Physics **143**, 224108 (2015); doi: 10.1063/1.4936408

View online: http://dx.doi.org/10.1063/1.4936408

View Table of Contents: http://scitation.aip.org/content/aip/journal/jcp/143/22?ver=pdfcov

Published by the AIP Publishing

The mean shape of transition and first-passage paths

Won Kyu Kim[a] and Roland R. Netz[b]
Department of Physics, Freie Universität Berlin, Arnimallee 14, 14195 Berlin, Germany

(Received 28 August 2015; accepted 12 November 2015; published online 9 December 2015)

Based on the one-dimensional Fokker-Planck equation in an arbitrary free energy landscape including a general inhomogeneous diffusivity profile, we analytically calculate the mean shape of transition paths and first-passage paths, where the shape of a path is defined as the kinetic profile in the plane spanned by the mean time and the position. The transition path ensemble is the collection of all paths that do not revisit the start position x_A and that terminate when first reaching the final position x_B. In contrast, a first-passage path can revisit its start position x_A before it terminates at x_B. Our theoretical framework employs the forward and backward Fokker-Planck equations as well as first-passage, passage, last-passage, and transition-path time distributions, for which we derive the defining integral equations. We show that the mean shape of transition paths, in other words the mean time at which the transition path ensemble visits an intermediate position x, is equivalent to the mean first-passage time of reaching the position x_A when starting from x without ever visiting x_B. The mean shape of first-passage paths is related to the mean shape of transition paths by a constant time shift. Since for a large barrier height U, the mean first-passage time scales exponentially in U, while the mean transition path time scales linearly inversely in U, the time shift between first-passage and transition path shapes is substantial. We present explicit examples of transition path shapes for linear and harmonic potentials and illustrate our findings by trajectories obtained from Brownian dynamics simulations. © *2015 AIP Publishing LLC.* [http://dx.doi.org/10.1063/1.4936408]

I. INTRODUCTION

For a reaction involving a free energy barrier, the ensemble of transition paths is defined as the collection of all paths that come from the reactant domain and enter the product domain for the first time without returning back to the boundary between the transition and reactant domains.[1–4] For continuous paths described by the Fokker-Planck (FP) equation, transition paths are generated by imposing absorbing boundary conditions on the boundaries between the product and transition domains as well as between the reactant and transition domains.[5] The mean transition path time τ^{TP} is the first moment of the transition path time distribution.[1] Based on an explicit formula derived by A. Szabo for the one-dimensional case,[5,6] τ^{TP} is for a large free energy barrier height U much shorter than Kramers' mean first-passage time τ^{KFP}. Note that according to Kramers, a first-passage path is allowed to revisit its origin many times and in the Fokker-Planck description is obtained by imposing a reflecting boundary condition close to the start position. By construction, a first-passage path is always terminated by a transition path, in other words, a transition path is the final segment of a first-passage path that does not return to its origin, for an illustration, see Fig. 1(a). In fact, while the mean first-passage time τ^{KFP} grows exponentially with the energy barrier height U, the mean transition path time τ^{TP} decreases linearly inversely in U for a fixed separation between the start and final positions along the one-dimensional reaction coordinate.[7] This means that in a reaction involving a large energy barrier, the system spends an exponential amount of time revisiting the reactant state, while the actual transition occurs very quickly.[8,9]

Although transition paths are crucial for the understanding of rare barrier-crossing events, they are in standard experiments that measure reaction rates not directly accessible. This situation dramatically changed with the advent of high resolution single molecule experiments that allow one to actually measure the mean folding and unfolding transition path times for proteins[10,11] as well as to estimate upper estimates for nucleic acid molecules.[12,13] Note that in these experiments, reaction paths are typically obtained from the FRET (fluorescence resonance energy transfer) efficiency between fluorophores connected to molecular positions that allow one to separate folded from unfolded states. As such, these experiments project the complex molecular dynamics onto a one-dimensional reaction coordinate that corresponds to an intramolecular distance, which motivated extensive work using models restricted to one-dimensional diffusion[14] (though it is clear that a projection into one dimension does not necessarily mean that a Markovian description by a Fokker-Planck equation is valid). Indeed, in single-molecule experiments, it is found that the mean transition path time is significantly smaller than the folding or unfolding time. In fact, the transition typically occurs so quickly that only estimates of the upper bound for the average transition path time of 200 μs for proteins[9] and 50 μs for nucleic acids[12] were obtained in experiments until both improvements in single molecule fluorescence time resolution and photon-by-photon analysis methods[15] have allowed average transition path times of less than 10 μs to be determined.[10,11]

[a]Electronic address: wkkim@physik.fu-berlin.de
[b]Electronic address: rnetz@physik.fu-berlin.de

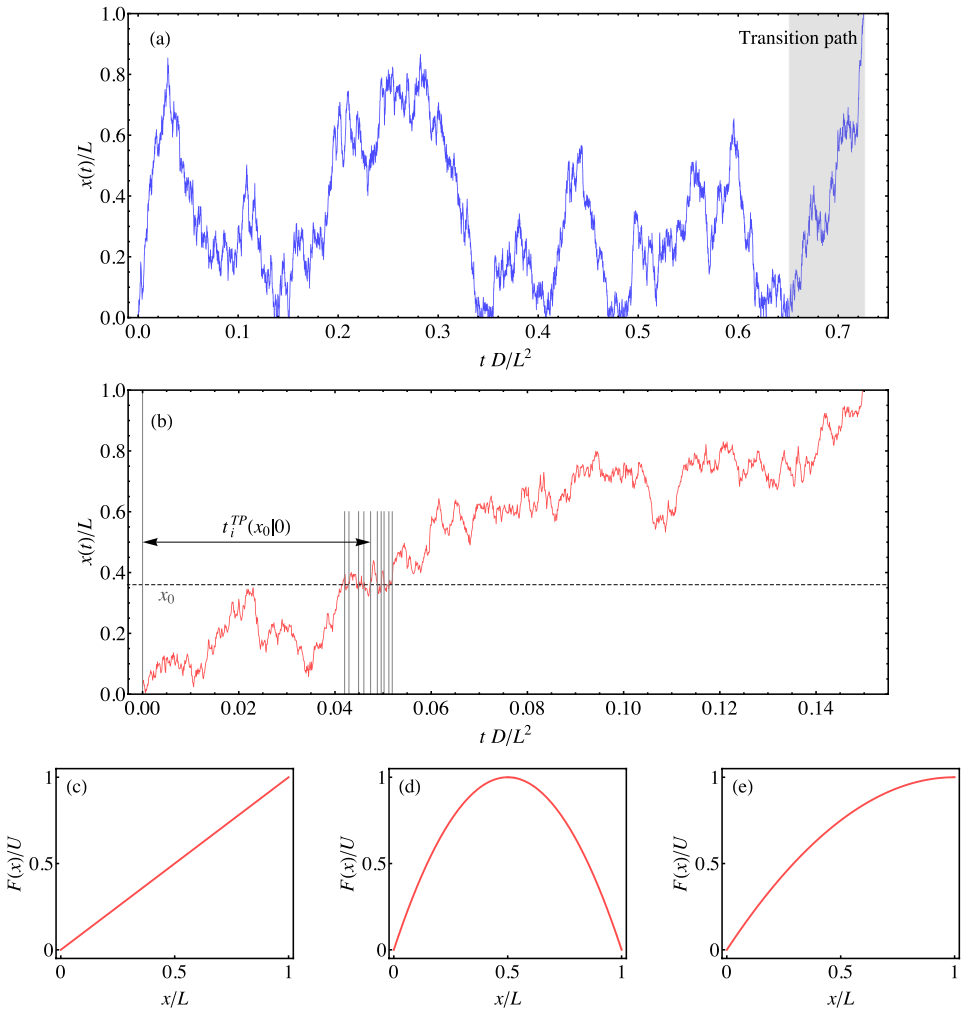

FIG. 1. (a) A typical first-passage path trajectory $x^{KFP}(t)$ for the force-free case in the presence of a reflecting boundary at $x=0$ and an absorbing boundary at $x=L$, obtained from Brownian dynamics (BD) simulations. The last part of the trajectory that does not return to the origin, indicated by the gray region, is a transition path. (b) A typical transition path trajectory $x^{TP}(t)$ for the force-free case, obtained from BD simulations. The times $t_i^{TP}(x_0|0)$ when the transition path crosses the position x_0 are indicated by vertical lines. (c)-(e) Model potentials $F(x)/U$ as function of the rescaled length x/L, where L is the transition length scale and U is the barrier height: (c) linear potential $F(x)=Ux/L$, (d) full harmonic potential $F(x)=4U(1-x/L)x/L$, and (e) harmonic ramp $F(x)=U(2-x/L)x/L$.

These experimental advances created theoretical interest in transition paths and led to intense simulation activities[16–18] as well as the development of analytical approaches.[7,19–21] In this work, we analytically derive the mean shape of transition and first-passage paths using a combination of the backward Fokker-Planck equation, the forward Fokker-Planck equation, and the renewal equation approach. We here define the mean shape of a path as the mean time at which a path visits a given position, as is appropriate for an ensemble of paths that are characterized by fixed start and end positions. Interestingly, first-passage and transition path shapes are identical modulo a shift by a constant time. This time shift corresponds to the residence time at the start position and is equivalent to the difference between the mean first-passage time and the mean transition path time. Shapes of transition paths and first-passage paths can directly be calculated from simulation trajectories and in principle also from experimental trajectories of sufficient time resolution. They are interesting because they contain much more information than mean transition path time or mean first-passage time alone and thus allow for a detailed characterization and test of the parameters and assumptions underlying the projection onto a one-dimensional reaction coordinate. Previous theoretical works on transition paths considered the mean step size of transition paths[1] or the mean position as a function of time for the sub-ensemble of transition paths with a given transition path time.[21] The advantage of our definition of the shape of a path is that it allows for an exact analytical solution for an arbitrary free energy profile.

Since the calculations leading to the expressions for the mean shape of transition paths (Sec. III) and of first-passage paths (Sec. IV) are rather lengthy, we in Sec. II present a short summary of our main findings. In Sec. V we show explicit results for shapes of transition and first-passage paths for constant, linear, and harmonic potentials. There we also demonstrate how to construct mean path shapes from trajectories that are generated using Brownian dynamics (BD) simulations.

II. SUMMARY OF MAIN RESULTS

Our one-dimensional diffusion model is defined by the Fokker-Planck operator in Eq. (6) for the motion of a particle in a one-dimensional free energy landscape $F(x)$ subjected to a diffusivity profile $D(x)$. The main results rest on a closed-form expression for the mean passage time $\tau^P(x|x_0)$, which we define as the mean time to reach the target position x when starting out from position x_0 while allowing for multiple recrossing events of x as well as x_0, see Eq. (41) for the definition of $\tau^P(x|x_0)$ in terms of moments of the Fokker-Planck Green's function. The derivation in Sec. III B employs the forward Fokker-Planck equation in the presence

of two exterior absorbing boundary conditions x_A and x_B, i.e., $x_A < x < x_B$ and $x_A < x_0 < x_B$. Our explicit results in Eq. (42) for $x_0 < x$ and in Eq. (43) for $x < x_0$ demonstrate that $\tau^P(x|x_0) = \tau^P(x_0|x)$, as expected based on reversibility. The mean first-passage times τ^{FP} follow from the mean passage times τ^P by moving the target position onto one of the absorbing boundaries,

$$\tau^{FP}(x_A|x_0) = \tau^P(x \to x_A|x_0) \tag{1}$$

and

$$\tau^{FP}(x_B|x_0) = \tau^P(x \to x_B|x_0). \tag{2}$$

The expressions obtained by this limiting procedure agree with our results, Eqs. (33) and (34), obtained in Sec. III A using the backward Fokker-Planck equation, which is the more common approach to calculate mean first-passage times. Likewise, the mean transition path time τ^{TP} follows from the mean first-passage time $\tau^{FP}(x_A|x_0)$ or $\tau^{FP}(x_B|x_0)$ by moving the start position onto the second absorbing boundary condition according to

$$\begin{aligned}\tau^{TP}(x_B|x_A) &= \tau^{FP}(x_B|x_0 \to x_A)\\ &= \tau^{TP}(x_A|x_B) = \tau^{FP}(x_A|x_0 \to x_B).\end{aligned} \tag{3}$$

The explicit result in Eq. (35) agrees with previous reports.[5]

The mean passage time $\tau^P(x_0|x_A)$ is the mean time at which a path starting from the absorbing boundary at x_A is present at position x_0. It turns out that $\tau^P(x_0|x_A)$ equals the mean time at which a transition path on its way from x_A to x_B is present at position x_0, which we define as the mean shape of a transition path, so that

$$\tau^{TP}_{shape}(x_0|x_A) = \tau^P(x_0|x_A) = \tau^{FP}(x_A|x_0), \tag{4}$$

where we used the symmetry of mean passage times so that $\tau^P(x_0|x_A) = \tau^P(x_A|x_0) = \tau^{FP}(x_A|x_0)$. Equation (4) constitutes one of our main results and shows that the transition path shape τ^{TP}_{shape} is identical to the mean first-passage time of reaching the absorbing boundary x_A from x_0 in the presence of a second absorbing boundary at x_B. The actual proof of Eq. (4) is presented in Sec. III C using a generalized renewal equation approach and involves the joint probability distribution $T(x_B,t;x,t'|x_A)$ that a transition path from x_A to x_B of length t is at time t' at position x, for which we present an explicit expression in Eq. (70).

Our definition of the mean shape of paths can also be applied to paths with different boundary conditions. In Sec. IV we derive the mean shape of Kramers first-passage paths $\tau^{KFP}_{shape}(x|x_0)$, which we define here as the ensemble of paths that start from x_0 in the vicinity of a reflecting boundary condition at x_A and reach an absorbing boundary at x_B. We find

$$\tau^{KFP}_{shape}(x|x_0) = \tau^{TP}_{shape}(x|x_0) + \tau^{KFP}_{\tilde{x}_A}(x_B|x_0) - \tau^{TP}(x_B|x_0), \tag{5}$$

where $\tau^{KFP}_{\tilde{x}_A}(x_B|x_0)$ denotes the mean first-passage time from a starting position x_0 to a final position x_B in the presence of a reflecting boundary condition at x_A. Equation (5) demonstrates that the mean shape of transition paths and the mean shape of Kramers first-passage paths are identical and shifted by a constant. As we show in Sec. V where we present results for explicit model potentials, transition path times are much shorter than first-passage times; consequently, the constant shift in Eq. (5) is significant.

III. DERIVATION OF TRANSITION PATH TIMES AND SHAPES

The FP operator is defined as[22–24]

$$\mathcal{L}(x) = \partial_x D(x) \mathrm{e}^{-F(x)} \partial_x \mathrm{e}^{F(x)}, \tag{6}$$

where $F(x)$ is the free energy in units of the thermal energy k_BT and $D(x)$ is the position-dependent diffusivity. In our previous analysis of protein folding trajectories from molecular dynamics simulations, we found that the diffusivity profile has a pronounced spatial dependence and together with the free energy profile allows one to predict kinetics that is rather insensitive to the precise definition of the reaction coordinate.[25] In fact, even for the simple system of two water molecules diffusing relative to each other in bulk liquid water, the diffusivity profile is not constant and therefore is important to take into account.[26] The Green's function can be formally written as

$$\mathcal{G}(x,t|x_0) = \mathrm{e}^{t\,\mathcal{L}(x)}\delta(x - x_0). \tag{7}$$

It fulfills the initial condition

$$\mathcal{G}(x,0|x_0) = \delta(x - x_0) \tag{8}$$

and solves the forward FP equation

$$\partial_t \mathcal{G}(x,t|x_0) = \mathcal{L}(x)\mathcal{G}(x,t|x_0). \tag{9}$$

The adjoint FP operator[22–24]

$$\mathcal{L}^\dagger(x_0) = \mathrm{e}^{F(x_0)} \partial_{x_0} D(x_0) \mathrm{e}^{-F(x_0)} \partial_{x_0} \tag{10}$$

defines the backward FP equation

$$\partial_t \mathcal{G}(x,t|x_0) = \mathcal{L}^\dagger(x_0)\mathcal{G}(x,t|x_0). \tag{11}$$

We will in Sec. III A first use the backward FP equation, as it allows one to derive transition path times and first-passage times in a most transparent and direct fashion. In Sec. III B, we will use the forward FP approach, which requires careful normalization of expectation values but allows one to calculate the more general mean passage times and from that various relations between mean transition path, first-passage, and passage times. Finally, in Sec. III C, we use the renewal equation approach to derive constitutive relations between transition path time, first-passage time, and last-passage time distributions. There we will be able to present a clear interpretation of the expressions in Eqs. (4) and (5) derived for the mean shape of transition and first-passage paths.

A. Backward Fokker-Planck approach

1. First-passage time distributions

The derivation in this section uses concepts and techniques presented previously in Refs. 23 and 24 and leads to Szabo's expression for the mean transition path time.[5,6] By assuming absorbing boundary conditions at positions x_A and x_B, we calculate first-passage times for paths that start at x_0

with $x_A < x_0 < x_B$ and reach the boundaries for the first time. For this, we define the survival probability

$$S(x_0,t) = \int_{x_A}^{x_B} \mathrm{d}x\, \mathcal{G}(x,t|x_0) \tag{12}$$

that the paths have not reached yet an absorbing boundary with the obvious properties $S(x_0,0) = 1$ and, for regular free energies, $S(x_0,\infty) = 0$. The first-passage distribution for reaching either one of the boundaries is defined as

$$K(x_A \vee x_B,t|x_0) = -\partial_t S(x_0,t), \tag{13}$$

and by using Eq. (9), it can be rewritten as

$$\begin{aligned} K(x_A \vee x_B,t|x_0) &= -\int_{x_A}^{x_B} \mathrm{d}x\, \mathcal{L}(x)\mathcal{G}(x,t|x_0) \\ &= \int_{x_A}^{x_B} \mathrm{d}x\, \partial_x j(x,t|x_0) \\ &= j(x_B,t|x_0) - j(x_A,t|x_0), \end{aligned} \tag{14}$$

where we use the flux at position x defined as

$$j(x,t|x_0) = -D(x)\mathrm{e}^{-F(x)}\partial_x \mathrm{e}^{F(x)}\mathcal{G}(x,t|x_0). \tag{15}$$

This shows that the total first-passage distribution can be decomposed into the two first-passage distributions $K(x_A,t|x_0) = -j(x_A,t|x_0)$ and $K(x_B,t|x_0) = j(x_B,t|x_0)$ corresponding to the respective boundary fluxes according to

$$K(x_A \vee x_B,t|x_0) = K(x_A,t|x_0) + K(x_B,t|x_0). \tag{16}$$

By applying the flux operator defined in Eq. (15) on both sides of backward FP Eq. (11), we obtain explicit equations for the first-passage distributions $K(x_A,t|x_0)$ and $K(x_B,t|x_0)$ as

$$\partial_t K(x_{A/B},t|x_0) = \mathcal{L}^\dagger(x_0)K(x_{A/B},t|x_0). \tag{17}$$

Defining the nth moments of the first-passage distributions as

$$K^{(n)}(x_{A/B}|x_0) = \int_0^\infty \mathrm{d}t\, t^n K(x_{A/B},t|x_0), \tag{18}$$

we obtain from Eq. (17) the set of equations

$$-nK^{(n-1)}(x_{A/B}|x_0) = \mathcal{L}^\dagger(x_0)K^{(n)}(x_{A/B}|x_0), \tag{19}$$

where we used the boundary condition $K(x_{A/B},t|x_0) = 0$ for $t = 0$ and $t = \infty$. Thus, all moments can be calculated recursively by straightforward integration of Eq. (19). The zeroth moment of the first-passage distribution is nothing but the committor or the splitting probability,

$$\phi_{A/B}(x_0) = K^{(0)}(x_{A/B}|x_0), \tag{20}$$

which gives the probability that a path starting at x_0 terminates at the boundary at x_A or x_B. From Eq. (19), we obtain for $n = 0$,

$$\mathcal{L}^\dagger(x_0)\phi_{A/B}(x_0) = 0. \tag{21}$$

From Eq. (13) and the boundary conditions $S(x_0,0) = 1$ and $S(x_0,\infty) = 0$, we conclude that $\int_0^\infty \mathrm{d}t\,[K(x_A,t|x_0) + K(x_B,t|x_0)] = 1$, in other words, the sum of the splitting probabilities is unity, eventually the path reaches a boundary,

$$\phi_A(x_0) + \phi_B(x_0) = 1. \tag{22}$$

For $n = 1$, we obtain from Eq. (19)

$$\mathcal{L}^\dagger(x_0)K^{(1)}(x_{A/B}|x_0) = -\phi_{A/B}(x_0). \tag{23}$$

Since the first-passage distributions $K^{(1)}(x_A|x_0)$ and $K^{(1)}(x_B|x_0)$ are not normalized, reflected by the fact that the splitting probabilities $\phi_{A/B}(x_0)$ are smaller than unity, the mean first-passage times are after normalization given by

$$\tau^{FP}(x_{A/B}|x_0) = \frac{K^{(1)}(x_{A/B}|x_0)}{\phi_{A/B}(x_0)}. \tag{24}$$

As a side remark, the mean first-passage time to reach either the boundary x_A or x_B is given by the sum of the first moments $\tau^{FP}(x_A \vee x_B|x_0) = K^{(1)}(x_A|x_0) + K^{(1)}(x_B|x_0)$. Adding the two equations for $K^{(1)}(x_A|x_0)$ and $K^{(1)}(x_B|x_0)$ in Eq. (23) and using that $\phi_A(x_0) + \phi_B(x_0) = 1$, we arrive at the familiar equation[23,24]

$$\mathcal{L}^\dagger(x_0)\tau^{FP}(x_A \vee x_B|x_0) = -1. \tag{25}$$

2. Splitting probabilities

We explicitly show the calculation of the splitting probabilities, all further calculations proceed similarly and are not detailed. We write Eq. (21) explicitly for $\phi_B(x_0)$,

$$\mathrm{e}^{F(x_0)}\partial_{x_0} D(x_0)\mathrm{e}^{-F(x_0)}\partial_{x_0}\phi_B(x_0) = 0. \tag{26}$$

Integrating once, we obtain

$$\frac{\mathrm{e}^{F(x)}}{D(x)} = C\partial_x \phi_B(x), \tag{27}$$

where C is an integration constant that will be determined later. Another integration yields

$$C^{-1}\int_{x_A}^{x_0} \mathrm{d}x\, \frac{\mathrm{e}^{F(x)}}{D(x)} = \phi_B(x)|_{x_A}^{x_0} = \phi_B(x_0), \tag{28}$$

where we used that $\phi_B(x_A) = 0$, i.e., a path that starts at the absorbing boundary at x_A will be immediately absorbed and the probability to reach x_B vanishes. Conversely, $\phi_B(x_B) = 1$ and thus

$$C = \int_{x_A}^{x_B} \mathrm{d}x\, \frac{\mathrm{e}^{F(x)}}{D(x)}. \tag{29}$$

For $\phi_A(x_0)$, we obtain

$$\phi_A(x_0) = 1 - \phi_B(x_0) = \frac{1}{C}\int_{x_0}^{x_B} \mathrm{d}x\, \frac{\mathrm{e}^{F(x)}}{D(x)}. \tag{30}$$

3. Mean first-passage times

From Eq. (23) and using the results for $\phi_A(x_0)$ and $\phi_B(x_0)$ in Eqs. (28) and (30), we can straightforwardly calculate the first moments of the first-passage distributions. The boundary conditions require some thought: The mean first-passage time to reach either absorbing boundaries, $\tau^{FP}(x_A \vee x_B|x_0) = K^{(1)}(x_A|x_0) + K^{(1)}(x_B|x_0)$, vanishes at the boundaries, i.e., $\tau^{FP}(x_A \vee x_B|x_A) = \tau^{FP}(x_A \vee x_B|x_B) = 0$. It follows that both first moments $K^{(1)}(x_A|x_0)$ and $K^{(1)}(x_B|x_0)$ must individually vanish at the absorbing boundaries, i.e., $K^{(1)}(x_A|x_A) = K^{(1)}(x_A|x_B) = 0$ and $K^{(1)}(x_B|x_A) = K^{(1)}(x_B|x_B) = 0$. With these boundary conditions, we obtain

$$K^{(1)}(x_A|x_0) = C\phi_B(x_0)\int_{x_0}^{x_B} \mathrm{d}x\, \mathrm{e}^{-F(x)}\phi_A^2(x) + C\phi_A(x_0)\int_{x_A}^{x_0} \mathrm{d}x\, \mathrm{e}^{-F(x)}\phi_A(x)\phi_B(x) \tag{31}$$

and

$$K^{(1)}(x_B|x_0) = C\phi_A(x_0)\int_{x_A}^{x_0} \mathrm{d}x\, \mathrm{e}^{-F(x)}\phi_B^2(x) + C\phi_B(x_0)\int_{x_0}^{x_B} \mathrm{d}x\, \mathrm{e}^{-F(x)}\phi_A(x)\phi_B(x). \tag{32}$$

From Eq. (24), the mean first-passage time to reach boundary A when starting from x_0 reads

$$\tau^{FP}(x_A|x_0) = C\frac{\phi_B(x_0)}{\phi_A(x_0)}\int_{x_0}^{x_B} \mathrm{d}x\, \mathrm{e}^{-F(x)}\phi_A^2(x) + C\int_{x_A}^{x_0} \mathrm{d}x\, \mathrm{e}^{-F(x)}\phi_A(x)\phi_B(x), \tag{33}$$

while the mean first-passage time to reach boundary B when starting from x_0 reads

$$\tau^{FP}(x_B|x_0) = C\frac{\phi_A(x_0)}{\phi_B(x_0)}\int_{x_A}^{x_0} \mathrm{d}x\, \mathrm{e}^{-F(x)}\phi_B^2(x) + C\int_{x_0}^{x_B} \mathrm{d}x\, \mathrm{e}^{-F(x)}\phi_A(x)\phi_B(x). \tag{34}$$

4. Transition path times

The transition path time denotes the mean time a path takes to reach from the absorbing boundary x_A to the other absorbing boundary at x_B and follows by the limiting procedure $\tau^{TP}(x_B|x_A) = \tau^{FP}(x_B|x_0 \to x_A)$. In the limit $x_0 \to x_A$, the first term in Eq. (34) vanishes and we obtain in agreement with Szabo's result[5]

$$\tau^{TP}(x_B|x_A) = C\int_{x_A}^{x_B} \mathrm{d}x\, \mathrm{e}^{-F(x)}\phi_A(x)\phi_B(x). \tag{35}$$

The same result is obtained from Eq. (33) by the limiting procedure $\tau^{TP}(x_A|x_B) = \tau^{FP}(x_A|x_0 \to x_B)$, reflecting that transition paths are reversible, i.e., $\tau^{TP}(x_B|x_A) = \tau^{TP}(x_A|x_B)$.

B. Forward Fokker-Planck approach

It is instructive to describe transition paths also using the forward FP equation[5] as this allows one to define passage and residence times and to derive various useful relations between transition path times, first-passage times, and passage times.

Defining moments of the Green's function as

$$\mathcal{G}^{(n)}(x|x_0) = \int_0^\infty \mathrm{d}t\, t^n \mathcal{G}(x,t|x_0), \tag{36}$$

we obtain from the forward FP Eq. (9) for $n > 0$ the recursive relations

$$-n\mathcal{G}^{(n-1)}(x|x_0) = \mathcal{L}(x)\mathcal{G}^{(n)}(x|x_0). \tag{37}$$

For $n = 0$, we obtain

$$-\delta(x - x_0) = \mathcal{L}(x)\mathcal{G}^{(0)}(x|x_0). \tag{38}$$

We again impose absorbing boundary conditions at x_A and x_B, i.e., $\mathcal{G}(x_A,t|x_0) = \mathcal{G}(x_B,t|x_0) = 0$, which means that all moments satisfy $\mathcal{G}^{(n)}(x_A|x_0) = \mathcal{G}^{(n)}(x_B|x_0) = 0$. Equations (37) and (38) are solved straightforwardly by integration, yielding

$$\mathcal{G}^{(0)}(x|x_0) = C\mathrm{e}^{-F(x)}\{\phi_A(x_0)\phi_B(x) - \theta(x - x_0)[\phi_A(x_0) - \phi_A(x)]\} \tag{39}$$

and

$$\mathcal{G}^{(1)}(x|x_0) = C\mathrm{e}^{-F(x)}\left\{\phi_A(x)\int_{x_A}^{x} \mathrm{d}x'\, \mathcal{G}^{(0)}(x'|x_0)\phi_B(x') + \phi_B(x)\int_{x}^{x_B} \mathrm{d}x'\, \mathcal{G}^{(0)}(x'|x_0)\phi_A(x')\right\}, \tag{40}$$

where $\theta(x - x_0)$ denotes the Heaviside function with the properties $\theta(x - x_0) = 1$ for $x > x_0$ and zero otherwise. Note that we assume the start and end positions x_0 and x of the paths to be inside the absorbing boundary conditions, i.e., $x_A < x < x_B$ and $x_A < x_0 < x_B$. The mean time to reach the position x when starting out from position x_0 follows from proper normalization as

$$\tau^P(x|x_0) = \frac{\mathcal{G}^{(1)}(x|x_0)}{\mathcal{G}^{(0)}(x|x_0)}, \tag{41}$$

we call this time the mean passage time and it is always larger than the mean first-passage time $\tau^{FP}(x|x_0)$ unless the target position x is an absorbing boundary. The mean passage time is the mean time to reach the target at position x, while allowing for multiple recrossing events. We obtain for $x_0 < x$ the result

$$\begin{aligned}\tau^P(x|x_0) = {} & C\frac{\phi_A(x_0)}{\phi_B(x_0)}\int_{x_A}^{x_0} \mathrm{d}x'\, \mathrm{e}^{-F(x')}\phi_B^2(x') \\ & + C\int_{x_0}^{x} \mathrm{d}x'\, \mathrm{e}^{-F(x')}\phi_A(x')\phi_B(x') \\ & + C\frac{\phi_B(x)}{\phi_A(x)}\int_{x}^{x_B} \mathrm{d}x'\, \mathrm{e}^{-F(x')}\phi_A^2(x'),\end{aligned} \tag{42}$$

while for $x < x_0$, we obtain

$$\tau^P(x|x_0) = C\frac{\phi_A(x)}{\phi_B(x)}\int_{x_A}^{x} dx'\, e^{-F(x')}\phi_B^2(x') + C\int_{x}^{x_0} dx'\, e^{-F(x')}\phi_A(x')\phi_B(x') + C\frac{\phi_B(x_0)}{\phi_A(x_0)}\int_{x_0}^{x_B} dx'\, e^{-F(x')}\phi_A^2(x'). \quad (43)$$

Obviously, the two expressions are connected by the symmetry $\tau^P(x|x_0) = \tau^P(x_0|x)$ that reflects the reversibility of the underlying processes described by the FP equation. We note that this symmetry also holds when x_0 and/or x are located on the absorbing boundaries x_A and x_B or when we shift the absorbing boundary conditions to infinity, i.e., for $x_A \to -\infty$ and/or $x_B \to \infty$, that is in the absence of absorbing boundary conditions.

As one can directly see, the mean first-passage times in Eqs. (33) and (34) follow from the passage times by the limiting procedures $\tau^{FP}(x_A|x_0) = \tau^P(x \to x_A|x_0)$ and $\tau^{FP}(x_B|x_0) = \tau^P(x \to x_B|x_0)$. The expression

$$\tau^P(x_0|x_0) = C\frac{\phi_A(x_0)}{\phi_B(x_0)}\int_{x_A}^{x_0} dx'\, e^{-F(x')}\phi_B^2(x') + C\frac{\phi_B(x_0)}{\phi_A(x_0)}\int_{x_0}^{x_B} dx'\, e^{-F(x')}\phi_A^2(x') \quad (44)$$

measures the mean time a path stays at the starting position x_0, we call this time the residence time. By explicit consideration of the results in Eqs. (33)–(35) and (44), it turns out that the transition path time $\tau^{TP}(x_B|x_A)$ in Eq. (35) is related to the sum of the first-passage times of reaching the absorbing boundaries at x_A and x_B from an intermediate position x_0 by subtracting the residence time,

$$\tau^{TP}(x_B|x_A) = \tau^{FP}(x_A|x_0) + \tau^{FP}(x_B|x_0) - \tau^P(x_0|x_0). \quad (45)$$

This shows that a transition path time can be constructed by adding the mean first-passage times of two paths starting at an arbitrary position x_0 that reach the boundaries x_A and x_B. Since each path recrosses the starting position, the residence time $\tau^P(x_0|x_0)$ has to be subtracted in order not to overcount these recrossing events. By a tedious but straightforward calculation, one can show that

$$\tau^{FP}(x_B|x_0) - \tau^P(x_0|x_0) = \tau^{TP}(x_B|x_0) = \tau^{TP}(x_0|x_B) \quad (46)$$

holds for the transition path time of going from x_0 to x_B or from x_B to x_0. Combining this with Eq. (45), we thus find

$$\tau^{TP}(x_A|x_B) = \tau^{FP}(x_A|x_0) + \tau^{TP}(x_0|x_B) = \tau^{TP}(x_A|x_0) + \tau^{TP}(x_B|x_0) + \tau^P(x_0|x_0). \quad (47)$$

The first line of Eq. (47) demonstrates that the transition path time from x_A to x_B can be decomposed into the first-passage time starting from an intermediate position x_0 and the transition path time continuing to the other boundary. Combining this with our definition for the shape of a transition path in Eq. (4), we conclude that

$$\tau^{TP}_{shape}(x_0|x_A) = \tau^{TP}(x_B|x_A) - \tau^{TP}(x_B|x_0) = \tau^{TP}(x_0|x_A) + \tau^P(x_0|x_0), \quad (48)$$

i.e., the mean shape of a transition path from x_A to x_0 is the transition path time from x_A to x_B minus the transition path time from x_0 to x_B, or, alternatively, the transition path from x_A to x_0 plus the residence time at x_0.

Finally, and as mentioned before, the symmetry of mean passage times $\tau^P(x|x_0) = \tau^P(x_0|x)$ also holds when we move the point x onto the absorbing boundary x_A, this turns the mean passage time $\tau^P(x_A|x_0)$ into the mean first-passage time and we obtain $\tau^{FP}(x_A|x_0) = \tau^P(x_0|x_A)$. Associating the transition path shape with the mean passage time of paths that start from the absorbing boundary x_A, we thus obtain $\tau^{TP}_{shape}(x_0|x_A) = \tau^P(x_0|x_A) = \tau^{FP}(x_A|x_0)$, as presented already in Eq. (4), which states that the transition path shape can alternatively be expressed as the first-passage time from x_0 to the boundary x_A. Note that Eqs. (45)-(48) have been explicitly derived in the presence of absorbing boundaries at positions x_A and x_B, we will show in Sec. III C that similar relation can be derived from integral equations for the distribution of passage times.

C. Renewal equation approach

1. First-passage time distribution

Relations between mean transition path times, first-passage times, and passage times can also be derived within the renewal equation approach without referral to an explicit underlying diffusive model. The relations derived in this section are thus more general than the previous derivations which were based on the one-dimensional FP equation. Also, the present derivation allows one to prove that the first-passage time $\tau^{FP}(x_A|x_0)$ in the presence of an absorbing boundary at x_B is identical to the shape of a transition path starting from x_A, $\tau^{TP}_{shape}(x_0|x_A)$, as presented in Eq. (4). In this section, we do not impose absorbing boundaries unless explicitly mentioned. Although we use a one-dimensional reaction coordinate, our results can be readily generalized to higher dimensions.

We start with the renewal equation[27,28]

$$\mathcal{G}(x,t|x_0) = \mathcal{G}_{x'}(x,t|x_0) + \int_0^t dt'\, \mathcal{G}(x,t-t'|x')K(x',t'|x_0), \quad (49)$$

where $\mathcal{G}_{x'}(x,t|x_0)$ denotes the Green's function in the presence of an absorbing boundary condition at x', which can be viewed as an alternative and more general definition of the first-passage time distribution $K(x,t|x_0)$ than the one presented in Eq. (17). The renewal equation states that the ensemble of all paths starting at time zero at x_0 and that are at position x at time t can be decomposed into paths that never reach the absorbing boundary condition at x' and paths that hit the boundary x' for the first time at time t' and from there on diffuse freely to x. By letting the position of x' coincide with x, we obtain the special case

$$\mathcal{G}(x,t|x_0) = \int_0^t dt'\, \mathcal{G}(x,t-t'|x)K(x,t'|x_0). \quad (50)$$

In terms of the Laplace transform

$$\tilde{\mathcal{G}}(x,\omega|x_0) = \int_0^\infty dt \mathcal{G}(x,t|x_0)e^{-\omega t},$$

Eq. (50) becomes

$$\tilde{\mathcal{G}}(x,\omega|x_0) = \tilde{\mathcal{G}}(x,\omega|x)\tilde{K}(x,\omega|x_0). \tag{51}$$

Using that moments can be calculated from the Laplace transform by taking derivatives according to

$$\mathcal{G}^{(n)}(x|x_0) \equiv \int_0^\infty dt\, t^n \mathcal{G}(x,t|x_0) = (-\partial_\omega)^n \tilde{\mathcal{G}}(x,\omega|x_0)|_{\omega=0}, \tag{52}$$

the normalized first moments are related by

$$-\partial_\omega \ln \tilde{K}(x,\omega|x_0)|_{\omega=0} = \frac{K^{(1)}(x|x_0)}{K^{(0)}(x|x_0)} = \frac{\mathcal{G}^{(1)}(x|x_0)}{\mathcal{G}^{(0)}(x|x_0)} - \frac{\mathcal{G}^{(1)}(x|x)}{\mathcal{G}^{(0)}(x|x)} \tag{53}$$

or

$$\tau^{FP}(x|x_0) = \tau^P(x|x_0) - \tau^P(x|x). \tag{54}$$

In other words, the mean first-passage time $\tau^{FP}(x|x_0)$ of going from x_0 to x in the absence of any additional absorbing or reflecting boundaries can be constructed from the mean passage time $\tau^P(x|x_0)$ of going from x_0 to x by subtracting the residence time $\tau^P(x|x)$ of staying at x. By symmetry of the passage time (derived in Sec. III B), we can write

$$\tau^{FP}(x|x_0) = \tau^P(x_0|x) - \tau^P(x|x). \tag{55}$$

This relation holds also in the presence of an absorbing boundary condition at x_0 (note that an absorbing boundary condition can be simply imposed by creating a potential well of infinite depth in the region $x < x_0$, which turns x_0 into an absorbing boundary for all paths that come from $x > x_0$). This turns $\tau^{FP}(x|x_0)$ into the transition path time $\tau^{TP}(x|x_0)$, the passage time $\tau^P(x_0|x)$ into the first-passage time $\tau^{FP}(x_0|x)$, and the residence time $\tau^P(x|x)$ without specified boundary conditions into the residence time at x in the presence of an absorbing boundary at x_0, which we denote by $\tau^P_{x_0}(x|x)$. We thus obtain from Eq. (55),

$$\tau^{TP}(x|x_0) = \tau^{TP}(x_0|x) = \tau^{FP}(x_0|x) - \tau^P_{x_0}(x|x), \tag{56}$$

which is equivalent to Eq. (46) (note that Eq. (46) by way of derivation holds in the presence of two absorbing boundary conditions at x_A and x_B, so to make the equivalence perfect we can either shift the boundary x_A in Eq. (46) to infinity or impose an additional absorbing boundary condition in Eq. (56)).

In order to derive Eq. (47), we need a convolution equation for first-passage times. For this, we choose in the renewal equation (49) the position x' to lie in the range $x_0 < x' < x$ and in this case obtain

$$\mathcal{G}(x,t|x_0) = \int_0^t \mathrm{d}t'\, \mathcal{G}(x,t-t'|x')K(x',t'|x_0). \tag{57}$$

We now impose an absorbing boundary condition at x, which turns both Green's functions into first-passage time distributions so that we obtain

$$K(x,t|x_0) = \int_0^t \mathrm{d}t'\, K(x,t-t'|x')K(x',t'|x_0), \tag{58}$$

valid for arbitrary positions x', with $x_0 < x' < x$. By using Laplace transformation, similarly as the calculation leading to Eq. (54), this yields

$$\tau^{FP}(x|x_0) = \tau^{FP}(x'|x_0) + \tau^{FP}(x|x'). \tag{59}$$

Imposing an additional absorbing boundary condition at x_0 turns this into

$$\tau^{TP}(x|x_0) = \tau^{TP}(x'|x_0) + \tau^{FP}_{x_0}(x|x'), \tag{60}$$

where the subindex x_0 in the last term indicates that an absorbing boundary is present at x_0. This is identical to Eq. (47), remembering that Eq. (47) was derived in the presence of an absorbing boundary at x_B. We next combine Eqs. (56) and (60) and obtain

$$\tau^{TP}(x|x_0) = \tau^{FP}_{x_0}(x|x') + \tau^{FP}(x_0|x') - \tau^P_{x_0}(x'|x'), \tag{61}$$

which is an equivalent Eq. (45) if we impose an additional absorbing boundary condition at x.

2. Transition path time distribution

We now impose an absorbing boundary condition at position x_0 in the convolution equation (58), this turns the two first-passage time distributions starting at x_0 into transition path time distributions, denoted by T, and we obtain

$$T(x,t|x_0) = \int_0^t \mathrm{d}t'\, K_{x_0}(x,t-t'|x')T(x',t'|x_0), \tag{62}$$

where $K_{x_0}(x,t-t'|x')$ is the first-passage time distribution with an additional absorbing boundary condition at x_0, with $x_0 < x' < x$. Note that Eq. (60) follows directly from this integral equation via Laplace transformation. Equation (62) means that a transition path can be decomposed into a transition path to an intermediate position x' followed by a first-passage path from x' that does not revisit x_0.

To go on with our derivation, we define the last-passage distribution H via the integral equation

$$\mathcal{G}(x,t|x_0) = \mathcal{G}_{x'}(x,t|x_0) + \int_0^t \mathrm{d}t'\, H(x,t-t'|x')\mathcal{G}(x',t'|x_0). \tag{63}$$

In essence, the last-passage distribution $H(x,t'|x')$ comprises all paths that go from x' to x without revisiting the starting point at x'. By moving the starting position x_0 to the position x', we obtain

$$\mathcal{G}(x,t|x') = \int_0^t \mathrm{d}t'\, H(x,t-t'|x')\mathcal{G}(x',t'|x'). \tag{64}$$

We now impose two absorbing boundary conditions, one at x and the other at x_0 with the condition $x_0 < x' < x$ and obtain

$$K_{x_0}(x,t|x') = \int_0^t \mathrm{d}t'\, T(x,t-t'|x')\mathcal{G}_{x_0,x}(x',t'|x'). \tag{65}$$

By inserting this integral equation into Eq. (62), we obtain

$$T(x,t|x_0) = \int_0^t \mathrm{d}t' \int_0^{t-t'} \mathrm{d}t''\, T(x,t-t'-t''|x') \times \mathcal{G}_{x_0,x}(x',t''|x')T(x',t'|x_0), \tag{66}$$

which has a nice intuitive interpretation: A transition path from x_0 to x can be decomposed into a transition path from x_0 to an arbitrary mid-point position x', a path that starts from x' and returns to x' without reaching the boundaries at x_0 and x, and finally a transition path from x' to the final destination x.

We now use the renewal equation (50) and impose an absorbing boundary condition at x_0 and replace the variable x by x' to yield

$$H(x',t|x_0) = \int_0^t \mathrm{d}t'\, \mathcal{G}_{x_0}(x',t-t'|x')T(x',t'|x_0), \quad (67)$$

which is an explicit integral equation for the last-passage time distribution. We now impose an additional absorbing boundary condition at x with the ordering $x_0 < x' < x$ and obtain

$$H_x(x',t|x_0) = \int_0^t \mathrm{d}t'\, \mathcal{G}_{x_0,x}(x',t-t'|x')T(x',t'|x_0). \quad (68)$$

By comparison with Eq. (66), we obtain

$$T(x,t|x_0) = \int_0^t \mathrm{d}t'\, T(x,t;x',t'|x_0), \quad (69)$$

where we define the joint distribution

$$T(x,t;x',t'|x_0) = T(x,t-t'|x')H_x(x',t'|x_0). \quad (70)$$

Equations (69) and (70), from which we will derive the transition path shape, have an intuitive interpretation: A transition path from x_0 to x can be decomposed into a last-passage path from x_0 to an arbitrary mid-point position x', followed by a transition path from x' to the final destination x. Note that the last-passage path from x_0 to x' does not visit the absorbing boundary condition x which is indicated by the subscript. By construction, $T(x,t;x',t'|x_0)$ is the joint probability that a transition path starting from x_0 and ending at x has a duration of t and is at time t' at the position x'. This interpretation follows from the fact that paths for times later than t' proceed on transition paths from x' to x and therefore do not visit back to x', consequently they do not contribute to the probability of being at x'.

The average shape of a transition path is obtained by averaging the joint distribution $T(x,t;x',t'|x_0)$ both over the intermediate time t' and the transition path duration t. We thus obtain for the shape of a transition path from x_A to x_B,

$$\tau^{TP}_{shape}(x|x_A) = \frac{\int_0^\infty \mathrm{d}t \int_0^t \mathrm{d}t'\, t' T(x_B,t;x,t'|x_A)}{\int_0^\infty \mathrm{d}t \int_0^t \mathrm{d}t'\, T(x_B,t;x,t'|x_A)}. \quad (71)$$

By slightly rearranging, we obtain

$$\tau^{TP}_{shape}(x|x_A) = \frac{\int_0^\infty \mathrm{d}t'\, t' H_{x_B}(x,t'|x_A)}{\int_0^\infty \mathrm{d}t'\, H_{x_B}(x,t'|x_A)} = \tau^{P}_{x_A,x_B}(x|x_A), \quad (72)$$

and thus have derived the important result that the shape of a transition path is given by the passage time from the absorbing boundary at x_A to position x in the presence of a second absorbing boundary at x_B, as presented in Eq. (4). We repeat that Eq. (4) shows that because of the symmetry of passage times, instead of averaging over paths that come from the absorbing boundary x_A, one can equally well average over first-passage paths that start from x and that end at the boundary x_A, the latter ensemble is for simulations much easier to implement and we will explicitly demonstrate the equivalence of both ensembles using our simulations results in Sec. V.

IV. THE SHAPE OF KRAMERS FIRST-PASSAGE PATHS

Here, we consider the mean shape of Kramers first-passage paths, defined as paths that start in the vicinity of a reflecting boundary and reach an absorbing boundary. We basically repeat the derivation steps from Sec. III C but replace the absorbing boundary condition at x_A, with $x_A < x_0 < x < x_B$ by a reflecting one. If we impose a reflecting boundary at position x_A in the convolution equation for the first-passage distribution Eq. (58), we obtain

$$K_{\tilde{x}_A}(x_B,t|x_0) = \int_0^t \mathrm{d}t'\, K_{\tilde{x}_A}(x_B,t-t'|x)K_{\tilde{x}_A}(x,t'|x_0), \quad (73)$$

where we denote a reflecting boundary condition by a subscript with a tilde and an adsorbing boundary condition by a subscript without a tilde.

We next impose an absorbing boundary condition at x_B and a reflecting boundary condition at x_A in the integral relation for the last-passage distribution in Eq. (64) and obtain

$$K_{\tilde{x}_A}(x_B,t|x) = \int_0^t \mathrm{d}t'\, T(x_B,t-t'|x)\mathcal{G}_{\tilde{x}_A,x_B}(x,t'|x). \quad (74)$$

By inserting this integral equation into Eq. (73), we obtain

$$K_{\tilde{x}_A}(x_B,t|x_0) = \int_0^t \mathrm{d}t' \int_0^{t-t'} \mathrm{d}t''\, T(x_B,t-t'-t''|x) \times \mathcal{G}_{\tilde{x}_A,x_B}(x,t''|x)K_{\tilde{x}_A}(x,t'|x_0), \quad (75)$$

which has a similar interpretation as the corresponding result for an absorbing boundary condition at the path origin in Eq. (66): A Kramers first-passage path from x_0 to x_B can be decomposed into a first-passage path from x_0 to an arbitrary mid-point position x, a path that starts from x and returns to x without reaching the absorbing boundary at x_B and without crossing the reflecting boundary at x_A, and finally a transition path from x to the final destination x_B.

We next impose an absorbing boundary condition at x_B and a reflecting boundary condition at x_A on the definition of the first-passage distribution in Eq. (50), from which we obtain

$$\mathcal{G}_{\tilde{x}_A,x_B}(x,t|x_0) = \int_0^t \mathrm{d}t'\, \mathcal{G}_{\tilde{x}_A,x_B}(x,t-t'|x)K_{\tilde{x}_A}(x,t'|x_0). \quad (76)$$

Comparison with Eq. (75) gives the integral equation

$$K_{\tilde{x}_A}(x_B,t|x_0) = \int_0^t \mathrm{d}t'\, T(x_B,t-t'|x)\mathcal{G}_{\tilde{x}_A,x_B}(x,t|x_0). \quad (77)$$

We now use similar arguments leading to our expression for the transition path shape in Eq. (72): The integrand in Eq. (77) is the joint probability that a first-passage path starting from x_0 and ending at x_B has a duration of t and is at time t' at position x. The average shape of a first-passage path from x_0 to x_B is obtained by averaging over both intermediate time t' and the first-passage path duration t, after some minor algebraic

manipulations, we thus obtain

$$\tau^{KFP}_{shape}(x|x_0) = \frac{\int_0^\infty \mathrm{d}t'\, t' \mathcal{G}_{\tilde{x}_A,x_B}(x,t'|x_0)}{\int_0^\infty \mathrm{d}t'\, \mathcal{G}_{\tilde{x}_A,x_B}(x,t'|x_0)} = \tau^{P}_{\tilde{x}_A,x_B}(x|x_0). \quad (78)$$

The only difference to the result for the transition path shape in Eq. (72) is that the absorbing boundary condition at the origin of the transition paths is replaced by a reflecting boundary condition at x_A.

By Laplace transformation of Eq. (77), we obtain (similarly as when we derived Eq. (54) from Eq. (50))

$$\tau^{KFP}_{\tilde{x}_A}(x_B|x_0) = \tau^{TP}(x_B|x) + \tau^{P}_{\tilde{x}_A,x_B}(x|x_0), \quad (79)$$

where we define the Kramers mean first-passage time $\tau^{KFP}_{\tilde{x}_A}(x_B|x_0)$ as the first moment of the first passage distribution $K_{\tilde{x}_A}(x_B,t|x_0)$ in Eq. (77), which is explicitly given by[29]

$$\tau^{KFP}_{\tilde{x}_A}(x_B|x_0) = \int_{x_0}^{x_B} \mathrm{d}x \frac{e^{F(x)}}{D(x)} \int_{x_A}^{x} \mathrm{d}x' e^{-F(x')} \quad (80)$$

and obeys $\tau^{KFP}_{\tilde{x}_A}(x_B|x_0) = \tau^{KFP}_{shape}(x_B|x_0)$. By combining Eqs. (48), (78), and (79), we find

$$\tau^{KFP}_{shape}(x|x_0) = \tau^{TP}_{shape}(x|x_0) + \tau^{P}_{\tilde{x}_A,x_B}(x_0|x_0), \quad (81)$$

showing that the mean shape of Kramers first-passage paths $\tau^{KFP}_{shape}(x|x_0)$ and the mean shape of transition paths $\tau^{TP}_{shape}(x|x_0)$ are identical and shifted by a constant given by $\tau^{P}_{\tilde{x}_A,x_B}(x_0|x_0)$. This shift corresponds to the residence time at the path origin x_0 and is according to Eq. (79) given by $\tau^{P}_{\tilde{x}_A,x_B}(x_0|x_0) = \tau^{KFP}_{\tilde{x}_A}(x_B|x_0) - \tau^{TP}(x_B|x_0)$.

V. RESULTS FOR EXPLICIT POTENTIALS

In this section, we present exemplary path shapes for a few different simple potential shapes shown in Figs. 1(c)-1(e). We consider a reaction coordinate x in the range $0 \le x \le L$, where L is the transition length scale, and restrict ourselves from now on to a homogeneous diffusion constant D. Note that an inhomogeneous diffusivity profile can be absorbed into a rescaled free energy profile via a rescaling of the reaction coordinate, employing the reparameterization invariance of the Fokker-Planck equation.[25] Choosing a constant D thus does not restrict the generality of the examples shown in a fundamental way.

A. Brownian dynamics simulations and trajectory analysis

We also demonstrate how to derive path shapes from trajectories obtained from one dimensional overdamped BD simulations. The simulations are based on the Langevin equation

$$\frac{\mathrm{d}x(t)}{\mathrm{d}t} = -D\frac{\mathrm{d}F(x)}{\mathrm{d}x} + \frac{\zeta(t)}{\gamma}, \quad (82)$$

where $\gamma = k_BT/D$ is the friction constant and $\zeta(t)$ is a Gaussian random force which fulfills $\langle\zeta(t)\rangle = 0$ and $\langle\zeta(t)\zeta(t')\rangle = 2\gamma k_BT\delta(t-t')$. The discretized and rescaled Langevin equation reads

$$\tilde{x}(\tilde{t}+\mathrm{d}\tilde{t}) = \tilde{x}(\tilde{t}) - \frac{\mathrm{d}F}{\mathrm{d}\tilde{x}}\mathrm{d}\tilde{t} + \sqrt{2\mathrm{d}\tilde{t}}\, r(\tilde{t}), \quad (83)$$

where $\tilde{x} = x/L$ is the rescaled position, $\tilde{t} = tD/L^2$ is the rescaled time, and $r(\tilde{t})$ is a Gaussian random number with zero mean and unit standard deviation. We iterate Eq. (83) with a typical time step $\mathrm{d}\tilde{t} = 10^{-4}$.

To obtain mean first-passage times $\tau^{FP}(0|x_0)$ and $\tau^{FP}(L|x_0)$, we vary the initial position from $x_0 = 0$ to $x_0 = L$ and measure the time needed to reach one of the two absorbing boundaries $x_A = 0$ or $x_B = L$ for the first time, we typically average over 10^5 first-passage times.

We also generate transition path trajectories within BD simulations. In practice, we initiate a trajectory at a reflecting boundary at $x = 0$ and record until it reaches the absorbing boundary at $x = L$, the transition path trajectory is the last section of the trajectory after it has last returned to the reflecting boundary at $x = 0$, as shown in Fig. 1(a). The mean transition path shape is obtained by the average

$$\tau^{TP}_{shape}(x_0|0) = \sum_{i=1}^{N} \frac{t_i^{TP}(x_0|0)}{N}, \quad (84)$$

where $t_i^{TP}(x_0|0)$ denotes the time at which a transition path trajectory that starts out at $x = 0$ crosses the position x_0, as illustrated in Fig. 1(b). Note that a single transition path crosses the position x_0 multiple times, the averaging in Eq. (84) is done over the entire transition path ensemble and over all crossing events, N thus counts the total number of crossing events in the entire transition path ensemble. For our final results, we typically generate 10^4 transition paths.

In a similar manner, we analyze Kramers first-passage trajectories, which start from a reflecting boundary at $x = 0$ and eventually reach the absorbing boundary at $x = L$, an example of which is shown in Fig. 1(a). To obtain the mean shape of Kramers first-passage trajectories, denoted by $\tau^{KFP}_{shape}(x_0|0)$, we calculate the average according to

$$\tau^{KFP}_{shape}(x_0|0) = \sum_{i=1}^{N} \frac{t_i^{KFP}(x_0|0)}{N}, \quad (85)$$

where $t_i^{KFP}(x_0|0)$ denotes the time at which a first-passage path that starts from $x = 0$ crosses $x = x_0$.

B. Force-free case

We first consider the force-free case, defined by a vanishing free energy $F = 0$. The splitting probabilities according to Eq. (30) read $\phi_A(x) = 1 - x/L$ and $\phi_B(x) = x/L$, and the transition path time according to Eq. (35) reads

$$\tau^{TP}(L|0) = \frac{L^2}{6D}, \quad (86)$$

which is three times smaller than Kramers mean first-passage time

$$\tau^{KFP}(L|0) = \frac{L^2}{2D}, \quad (87)$$

according to Eq. (80). This is due to the fact that the Kramers first-passage trajectories return to the origin many times, as illustrated in Fig. 1(a).

The normalized distribution functions for the transition path time $\tau^{TP}(L|0)$ (circles) and the Kramers first-passage

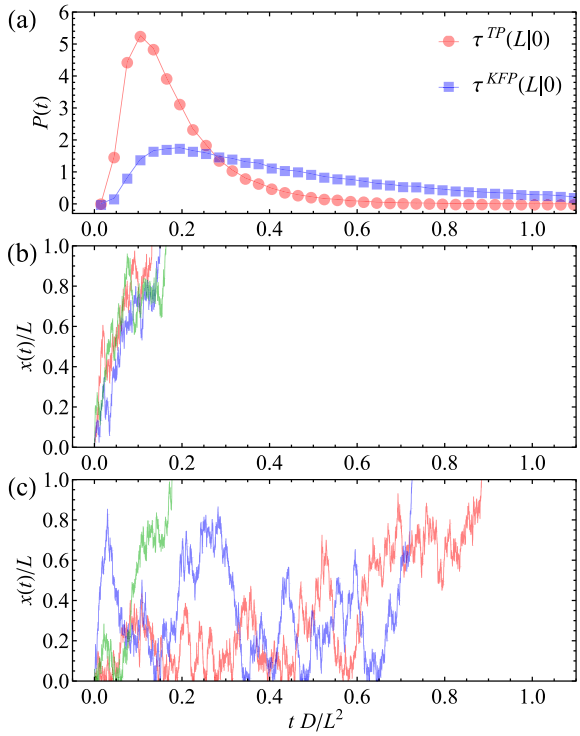

FIG. 2. (a) The normalized distribution functions for the transition path time $\tau^{TP}(L|0)$ (circles) and the Kramers first-passage time $\tau^{KFP}(L|0)$ (squares) in the force-free case, obtained from BD simulations. (b) Three typical transition path trajectories $x(t)$. (c) Three typical Kramers first-passage trajectories $x(t)$.

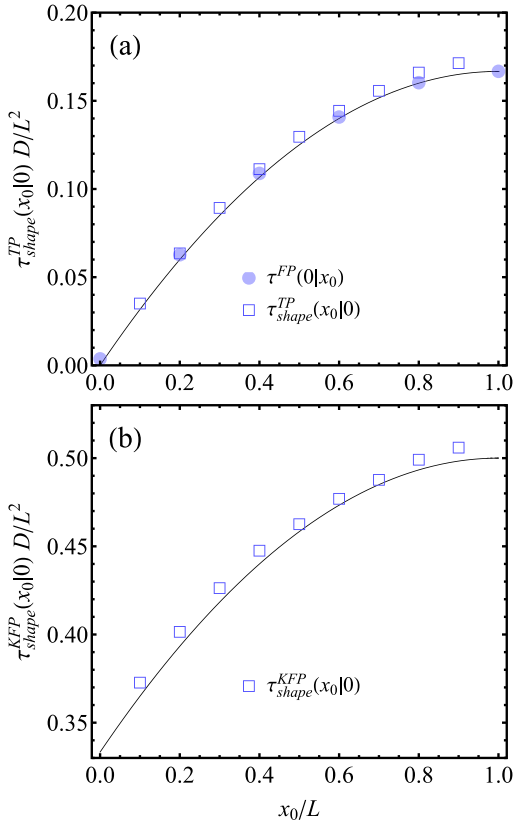

FIG. 3. (a) Mean shape of transition paths $\tau^{TP}_{shape}(x_0|0)$ in the force-free case. The solid line shows the analytic result in Eq. (88). Filled circles show BD simulation results for the mean first-passage time $\tau^{FP}(0|x_0)$, while open squares show the mean shape from the analysis of transition paths according to Eq. (84). (b) Mean shape of Kramers first-passage paths $\tau^{KFP}_{shape}(x_0|0)$ in the force-free case. Symbols show BD simulation results, while the solid line shows analytic results according to Eqs. (81) and (88). Note that the two curves in (a) and (b) are identical except a vertical shift by a constant time.

time $\tau^{KFP}(L|0)$ (squares) are shown in Fig. 2(a), obtained from BD simulations. The transition path time distribution is more sharply peaked compared with the Kramers first-passage time distribution, in agreement with previous numerical and analytical results[19] and as directly reflected by the trajectories shown in Figs. 2(b) and 2(c).

The mean transition path shape is, according to Eqs. (33) and (4), given as

$$\tau^{TP}_{shape}(x_0|0) = \tau^{FP}(0|x_0) = \frac{Lx_0}{6D}\left(2 - \frac{x_0}{L}\right) \tag{88}$$

and is depicted in Fig. 3(a) by a solid line. Note that the transition path shape is a quadratic function, transition paths start out with finite slope at the origin and reach the final destination with vanishing slope. Regarding the path velocity, which can be interpreted as the inverse function, i.e., position versus mean time, the mean path has a diverging velocity at the final position. This pronounced asymmetry, which is a universal property of mean transition path shapes for all potentials, can be easily understood by considering the first line of Eq. (48): Since the mean transition path time $\tau^{TP}(x_B|x_0)$ in Eq. (48) scales quadratically in $x_B - x_0$, the transition path shape approaches its final position with a vanishing slope. The filled symbols in Fig. 3(a) show the BD simulation results for the first-passage time $\tau^{FP}(0|x_0)$, while the open square symbols show the BD results for $\tau^{TP}_{shape}(x_0|0)$ obtained from actual transition path trajectories via Eq. (84), both simulation results agree well with the theoretical result in Eq. (88).

The solid curve in Fig. 3(b) shows the Kramers mean first-passage shape $\tau^{KFP}_{shape}(x_0|0)$, calculated from Eqs. (81) and (88). The Kramers mean first-passage shape $\tau^{KFP}_{shape}(x_0|0)$ is, according to Eqs. (79) and (81), identical to the transition path shape $\tau^{TP}(x_0|0)$ shifted by the amount $\tau^{P}_{\tilde{x}_A=0,x_B=L}(0|0) = \tau^{KFP}(L|0) - \tau^{TP}(L|0) = L^2/(3D)$. The symbols in Fig. 3(b) show the BD results using Eq. (85), again, the agreement is very good.

C. Linear potential

For a linear potential $F = Ux/L$, we find from Eq. (35) for the transition path time

$$\tau^{TP}(L|0) = \frac{L^2}{D}\frac{U\coth\left(\frac{U}{2}\right) - 2}{U^2}, \tag{89}$$

which is even in U. This means that the transition path time is the same irrespective of whether the transition paths go up the linear potential or whether they go down. This of course follows directly from the general symmetry of passage times in Eqs. (42) and (43). To leading order in U, the asymptotic behavior reads

$$\tau^{TP}D/L^2 \approx \begin{cases} \frac{1}{6} - \frac{U^2}{360}, & |U| \ll 1, \\ 1/|U|, & |U| \gg 1. \end{cases} \tag{90}$$

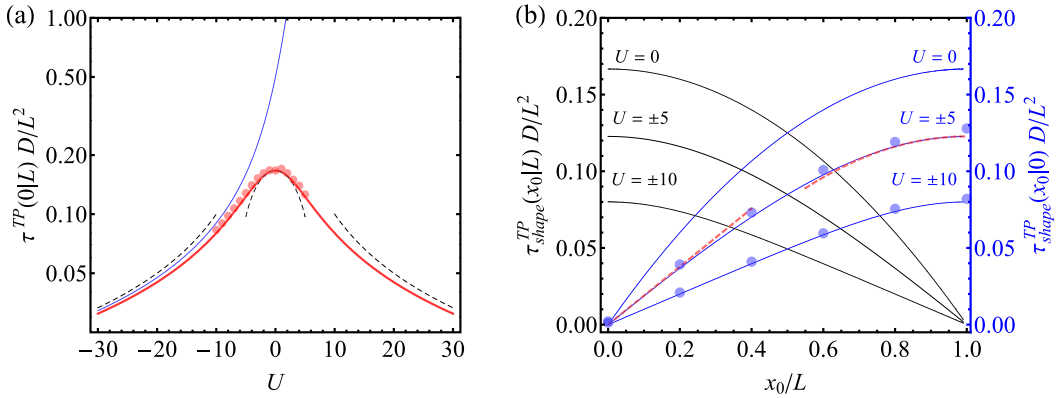

FIG. 4. Results for a linear potential $F = Ux/L$. (a) The solid red curve shows the mean transition path time $\tau^{TP}(0|L)$ from Eq. (89) as a function of U on a log-linear scale. The broken curves depict the asymptotic expressions from Eq. (90). For comparison, the solid blue curve shows Kramers mean first-passage time $\tau^{KFP}(L|0)$ which monotonically increases with U. The symbols denote BD simulation results. (b) Mean shapes of transition paths τ^{TP}_{shape}. Blue curves depict $\tau^{TP}_{shape}(x_0|0)$ starting from the left boundary from Eq. (91), while black curves depict $\tau^{TP}_{shape}(x_0|L)$ starting from the right boundary from Eq. (92). Symbols denote BD simulation results for $U = -5$ and $U = -10$, while broken red curves depict the asymptotic expressions for $U = \pm 5$ from Eq. (93).

The red solid curve in Fig. 4(a) shows $\tau^{TP}(L|0)$ in Eq. (89), while the asymptotic expressions in Eq. (90) are depicted by broken curves. Note that the Kramers mean first-passage time according to Eq. (80) $\tau^{KFP}(L|0) = L^2(e^U - 1 - U)/(DU^2)$, shown by a solid blue curve in Fig. 4(a), shows a very different behavior and in particular is a monotonically increasing function of U. For large potential strength $U \gg 1$, we find an exponential increase to leading order, $\tau^{KFP}(L|0) \sim e^U/U^2$. The symbols in Fig. 4(a) show BD simulation results for the transition path time, which agree well with the theory.

A further noteworthy fact is that the mean transition path time τ^{TP} is for non-zero values of U strictly smaller than the force-free result $\tau^{TP} = L^2/(6D)$ corresponding to the maximum value obtained for $U = 0$. This means that transition paths in a linear potential are faster than force-free transition paths, regardless of whether the slope is positive or negative.

The transition path shapes according to Eqs. (33) and (4) read

$$\tau^{TP}_{shape}(x_0|0) = \frac{L^2}{D}\frac{\operatorname{csch}\left(\frac{U}{2}\right)\operatorname{csch}\left(\frac{U}{2}-\frac{Ux_0}{2L}\right)\left[(x_0/L-2)\sinh\left(\frac{Ux_0}{2L}\right)+\frac{x_0}{L}\sinh\left(U-\frac{Ux_0}{2L}\right)\right]}{2U}, \tag{91}$$

$$\tau^{TP}_{shape}(x_0|L) = \frac{L^2}{D}\frac{\coth(U/2)-\frac{x_0}{L}\coth(\frac{Ux_0}{2L})}{U}, \tag{92}$$

where $\tau^{TP}_{shape}(x_0|0)$ has the asymptotic limits

$$\tau^{TP}_{shape}(x_0|0)D/L^2 \approx \begin{cases} \dfrac{U-\sinh U}{U(1-\cosh U)}\dfrac{x_0}{L}, & x_0 \ll L, \\ \tau^{TP}(L|0)D/L^2 - \dfrac{1}{6}(\dfrac{x_0}{L}-1)^2, & x_0 \approx L. \end{cases} \tag{93}$$

Figure 4(b) shows the transition path shapes, where the blue curves depict $\tau^{TP}_{shape}(x_0|0)$ starting from the left in Eq. (91) and the black curves depict $\tau^{TP}_{shape}(x_0|L)$ starting from the right in Eq. (92). Symbols denote BD simulation results for $U = -5$ and $U = -10$. The broken red curves depict the asymptotic limits in Eq. (93) for $U = \pm 5$. Due to the simple potential form, the shapes τ^{TP}_{shape} are symmetric with respect to an exchange of starting positions.

D. Harmonic potential

For a harmonic potential $F = 4Ux(1 - x/L)/L$, we find from Eq. (35) for the transition path time

$$\tau^{TP}(L|0) = \frac{L^2}{4D}F_{2,2}(-U) - \frac{L^2}{2D\sqrt{\pi}U\operatorname{erf}(\sqrt{U})}\int_0^{\sqrt{U}} \mathrm{d}y\ y^2 e^{-y^2}F_{2,2}(-y^2), \tag{94}$$

where $F_{2,2}(x) = F_{2,2}(\{1,1\};\{3/2,2\};x)$ is the generalized hypergeometric function. For the small barrier limit $|U| \ll 1$, we find to leading order

$$\tau^{TP}(L|0) \approx \frac{L^2}{D}\left[\frac{1}{6} - \frac{2}{45}U\right], \tag{95}$$

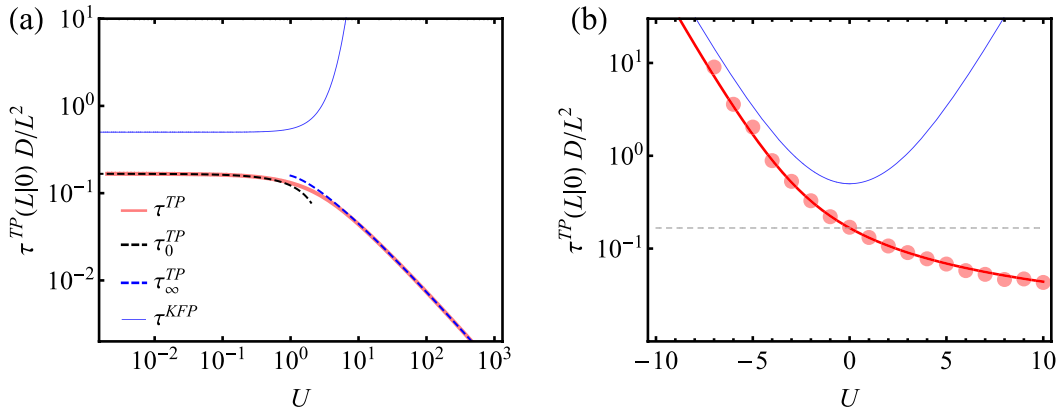

FIG. 5. Results for the harmonic potential $F = 4Ux(1-x/L)/L$ as a function of the barrier height U. (a) Mean transition path time $\tau^{TP}(L|0)$ from Eq. (94) (solid red curve) on a log-log scale, compared with the asymptotic expressions in Eqs. (95) and (96) (dashed lines). (b) Mean transition path time $\tau^{TP}(L|0)$ (solid red curve) on a log-linear scale compared with BD simulation data (symbols). Solid blue curves depict the Kramers mean first-passage time $\tau^{KFP}(L|0)$ from Eq. (98). The horizontal dashed line depicts the force-free transition path time $\tau^{TP} = L^2/(6D)$.

which linearly deviates from the force-free transition path time $\tau^{TP} = L^2/(6D)$. For the large barrier limit $U \to \infty$, we recover the known asymptotic result[7,9]

$$\tau^{TP}(L|0) \approx \frac{L^2 \ln(2e^\gamma U)}{8DU}, \tag{96}$$

where $\gamma \approx 0.577$ is the Euler gamma constant, and we used $\mathrm{erf}(\sqrt{U}) \approx 1$, $F_{2,2}(-U) \approx \ln(4e^\gamma U)/(2U)$ and $\int_0^\infty \mathrm{d}y\ y^2 e^{-y^2} F_{2,2}(-y^2) = (\sqrt{\pi}/4)\ln(2)$ for large U. We note that the denominator $8U$ in Eq. (96) can be reinterpreted as the curvature $\omega^2 = \left|(\mathrm{d}^2F/\mathrm{d}x^2)_{x=L/2}\right|$ at the barrier top of the harmonic potential, yielding the previously published form[9]

$$\tau^{TP}(L|0) \approx \frac{\ln(2e^\gamma U)}{D\omega^2}. \tag{97}$$

For fixed potential curvature and varying potential height, Eq. (97) shows that the transition path time increases logarithmically with increasing potential height U, while for fixed diffusion length L, Eq. (96) shows that the transition path time to leading order decreases inversely linearly with increasing potential height U.[7]

In Fig. 5, we present $\tau^{TP}(L|0)$ as a function of the barrier height U. In Fig. 5(a), we show $\tau^{TP}(L|0)D/L^2$ from Eq. (94) on a log-log scale (solid red curve), which is seen to decrease from the force-free case $\tau^{TP}D/L^2 = 1/6$ as U increases. We also show the asymptotic expressions in Eqs. (95) and (96) by dashed curves. In Fig. 5(b), we show $\tau^{TP}(L|0)$ from Eq. (94) on a log-linear scale (solid red curve), here we also compare with BD simulation results obtained via Eq. (84). The solid blue curves in Fig. 5 depict the Kramers mean first-passage time according to Eq. (80) and given by

$$\tau^{KFP}(L|0) = \frac{L^2}{D}\frac{\pi \mathrm{erf}\left(\sqrt{U}\right)\mathrm{erfi}\left(\sqrt{U}\right)}{8U}, \tag{98}$$

where $\mathrm{erf}(x) = \frac{2}{\sqrt{\pi}}\int_0^x e^{-t^2}\mathrm{d}t$ is the error function, and $\mathrm{erfi}(x) = \frac{2}{\sqrt{\pi}}\int_0^x e^{t^2}\mathrm{d}t$ is the imaginary error function. The leading order result for large $|U|$ reads

$$\tau^{KFP}(L|0)D/L^2 = \frac{\sqrt{\pi}}{8}\frac{e^{|U|}}{|U|^{3/2}}. \tag{99}$$

In Fig. 5, we see that the transition path time $\tau^{TP}(L|0)$ is a monotonically decreasing function of the barrier height U, while the Kramers time $\tau^{KFP}(L|0)$ is a symmetric function

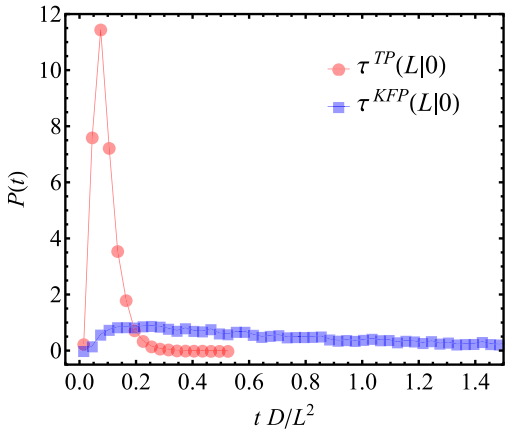

FIG. 6. Normalized distribution functions for the transition path time $\tau^{TP}(L|0)$ (circles) and the Kramers first-passage time $\tau^{KFP}(L|0)$ (squares) for a harmonic barrier with $U = 3$, obtained from BD simulations.

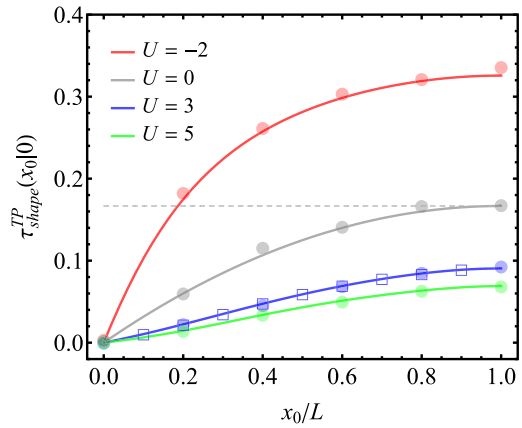

FIG. 7. Mean transition path shape $\tau^{TP}_{shape}(x_0|0)$ from Eq. (100), for different values of the barrier height U of the harmonic potential $F = 4Ux(1-x/L)/L$. Symbols show BD simulation results for $\tau^{FP}(0|x_0)$ (filled spheres) and $\tau^{TP}_{shape}(x_0|0)$ (open squares) for $U = 3$. The horizontal dashed line depicts the force-free transition path time $\tau^{TP} = L^2/(6D)$.

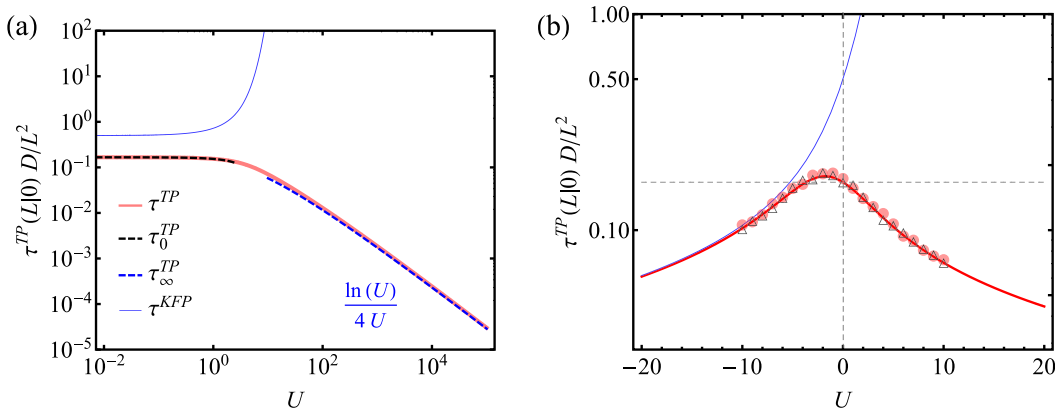

FIG. 8. Results for the harmonic ramp $F(x) = Ux(2-x/L)/L$. (a) Mean transition path time $\tau^{TP}(L|0)$ from Eq. (101) (solid red curve) on a log-log scale, asymptotic expression Eqs. (102) and (103) are shown by dashed black lines. The blue line shows Kramers mean first-passage time $\tau^{KFP}(L|0)D/L^2$ from Eq. (104). (b) Same curves shown on a log-linear scale, compared with BD simulation data for transition paths starting from the left, $\tau^{TP}(L|0)$ (circles) and for transition paths starting from the right, $\tau^{TP}(0|L)$ (triangles). The horizontal dashed line depicts the force-free transition path time $\tau^{TP}(L|0)D/L^2 = 1/6$.

and has a minimum of $\tau^{KFP} = L^2/(2D)$ at $U = 0$. In fact, transition paths over a harmonic barrier with $U > 0$ are faster, while transition paths through a harmonic well characterized by $U < 0$ are slower compared to the force-free case, with $U = 0$. This can be rationalized by Eq. (47), since the transition path time for reaching from the boundaries to the center of the harmonic potential is rather insensitive on whether U is positive or negative (as will be shown in Sec. V E), but the residence time at the center of the harmonic potential is much larger for the case of a harmonic well with $U < 0$ than for a harmonic barrier with $U > 0$. The symmetric behavior of the Kramers mean first-passage time can be understood based on Eq. (59) since first-passage time are transitive: The first-passage time for traversing a harmonic potential is the sum of the first-passage times from the boundary to the middle and from the middle to the other boundary. We reiterate that mean first-passage times are transitive, as shown in Eq. (59), while transition path times are not, as shown in Eq. (47).

In Fig. 6, we show the normalized distribution functions for the transition path time (circles) and for the Kramers first-passage time (squares) for $U = 3$, obtained from BD simulations. The transition path time distribution shows a pronounced peak around $\tau D/L^2 = 0.1$, close to the mean transition path time $\tau^{TP}(L|0)(U = 3)D/L^2 \approx 0.1$, as seen in Fig. 5. In contrast, the Kramers first-passage time distribution is quite broad, the first moment is given by $\tau^{KFP}(L|0)(U = 3)D/L^2 \approx 1$ and thus is 10 times larger than the mean transition path time.

For the transition path shape, we find according to Eqs. (33) and (4),

$$\tau^{TP}_{shape}(x_0|0) = \tau^{TP}(L|0) - \frac{L^2}{2DU}\int_{\sqrt{U}}^{\sqrt{U}(2x_0/L-1)} \mathrm{d}y \left(\frac{\mathrm{erf}(y) - \mathrm{erf}(\sqrt{U})}{\mathrm{erf}(\sqrt{U}(2x_0/L-1)) - \mathrm{erf}(\sqrt{U})} - \frac{1}{2}\right) D_+(y), \tag{100}$$

where $D_+(x) = e^{-x^2}\int_0^x \mathrm{d}t e^{t^2}$ is the Dawson integral function. The second term in Eq. (100) vanishes for $x_0 = L$ and reduces to $-\tau^{TP}(L|0)$ given in Eq. (94) for $x_0 = 0$.

Figure 7 depicts the mean transition path shapes $\tau^{TP}_{shape}(x_0|0)$ in Eq. (100) for different values of the barrier height U. Transition paths are faster for positive values of U, i.e., for paths that go over a harmonic barrier top, while they are slower for negative values of U, i.e., for paths that traverse a harmonic well. Again, we observe a pronounced asymmetry of the mean shape of transition paths, paths start out with finite slope and reach the boundary at $x = L$ with vanishing slope. Filled symbols show BD simulation results for $\tau^{FP}(0|x_0)$, while open symbols show BD simulation results for $\tau^{TP}_{shape}(x_0|0)$ from the transition path ensemble for $U = 3$. We observe good agreement between the two different ways of extracting transition path shapes from simulation trajectories, as expected based on our analytical results, as well as with our analytically derived shape.

E. Harmonic ramp

Here, we consider the harmonic potential $F(x) = Ux(2 - x/L)/L$ which has a barrier top $F = U$ at the final position $x = L$.

The transition path time reads

$$\tau^{TP}(L|0) = \frac{L^2\int_0^{\sqrt{U}} \mathrm{d}y\ y^2 e^{-y^2} F_{2,2}(y^2)}{D\sqrt{\pi}U\,\mathrm{erf}(\sqrt{U})}. \tag{101}$$

For small U, we find the asymptotic expression

$$\tau^{TP}(L|0)\,D/L^2 \approx \frac{1}{6} - \frac{U}{90} - \frac{2U^2}{945}, \tag{102}$$

while for large U, we find

$$\tau^{TP}(L|0)\,D/L^2 \approx \frac{\ln U}{4U}. \tag{103}$$

Figure 8 depicts $\tau^{TP}(L|0)$ as function of the barrier height U. In Fig. 8(a), we show, on a double logarithmic scale, the numerically integrated $\tau^{TP}(L|0)$ from Eq. (101) by the solid red curve and compare with the asymptotic expressions Eqs. (102) and (103) (dashed curves). In Fig. 8(b), we show $\tau^{TP}(L|0)$ from Eq. (101) on a log-linear scale, the symbols show BD simulation results. The solid blue curves in Fig. 8 depict the Kramers mean first-passage time, which is given by

$$\tau^{KFP}(L|0) = \frac{L^2}{D}\left[\frac{\pi \mathrm{erf}\left(\sqrt{U}\right)\mathrm{erfi}\left(\sqrt{U}\right)}{4U} - \frac{F_{2,2}(-U)}{2}\right] \tag{104}$$

and has the leading order expression

$$\tau^{KFP}(L|0) = \frac{\sqrt{\pi}L^2}{4D}\frac{e^U}{U^{3/2}}, \tag{105}$$

for large U.

The transition path time $\tau^{TP}(L|0)D/L^2$ is nonmonotonic and is maximal for finite U around $U \approx -21/8$, implying that transition paths that move down a weak harmonic ramp are slower than in the force-free case. For large $|U|$, $\tau^{TP}(L|0)$ decreases, similar to the linear potential case shown in Fig. 4(a). In contrast, the Kramers mean first-passage time $\tau^{KFP}(L|0)$ exponentially increases as U increases.

For the transition path shapes, we find according to Eqs. (33) and (4),

$$\tau^{TP}_{shape}(x_0|0) = \tau^{TP}(L|0) - \frac{\sqrt{\pi}L^2}{2DU}\int_0^{y_0} dy e^{y^2}\mathrm{erf}(y)\left[1 + \frac{\mathrm{erf}(y)}{\mathrm{erf}(y_0)} - 2\frac{\mathrm{erf}(y)}{\mathrm{erf}(\sqrt{U})}\right], \tag{106}$$

$$\tau^{TP}_{shape}(x_0|L) = \tau^{TP}(L|0) - \frac{\sqrt{\pi}L^2}{2DU}\int_{y_0}^{\sqrt{U}} dy e^{y^2}\frac{\left[\mathrm{erf}(\sqrt{U}) - \mathrm{erf}(y)\right]\left[\mathrm{erf}(y_0) - \mathrm{erf}(y)\right]}{\mathrm{erf}(y_0) - \mathrm{erf}(\sqrt{U})}, \tag{107}$$

where $y_0 \equiv \sqrt{U}(1 - x_0/L)$.

Figure 9 depicts the transition path shapes starting from the left, $\tau^{TP}_{shape}(x_0|0)$ (solid curves) from Eq. (106), and starting from the right, $\tau^{TP}_{shape}(x_0|L)$ (broken curves) from Eq. (107), for different values of the barrier height U. The symbols show the corresponding results from BD simulations. Note that the transition path shapes $\tau^{TP}_{shape}(x_0|0)$ and $\tau^{TP}_{shape}(x_0|L)$ at constant U are asymmetric with respect to the exchange of start and end positions, due to the asymmetry of the barrier potential (this becomes clear by comparing the mean shapes for $U = 0$ (grey line) and for $U = -5$ (red line) starting from the left boundary and starting from the right boundary).

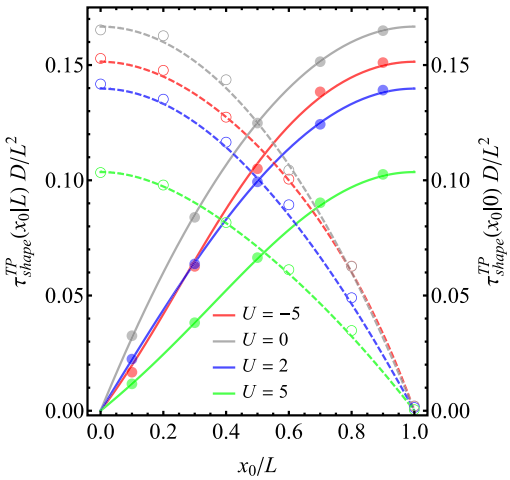

FIG. 9. Mean transition path shapes starting from the left, $\tau^{TP}_{shape}(x_0|0)$ (solid curves) from Eq. (106) and mean transition path shapes starting from the right, $\tau^{TP}_{shape}(x_0|L)$ (broken curves) from Eq. (107), for different values of the barrier height U of the harmonic ramp $F(x) = Ux(2 - x/L)/L$. The symbols show the corresponding BD simulation results.

VI. CONCLUSION

Based on the one-dimensional Fokker-Planck equation, we develop the theoretical formalism to calculate mean shapes of transition paths and of Kramers first-passage paths for arbitrary free energy and diffusivity landscapes. We use a combination of the backward and forward Fokker Planck approaches to derive explicit expressions for transition and first-passage path shapes. For the interpretation of our results for the mean shapes, we present convolution expressions for the distribution functions of transition, first-passage and passage times. We show that the mean shape of Kramers first-passage paths is identical to the shape of transition paths shifted by a constant. Based on our analytic theory, we present mean shapes for several simple model potentials. We illustrate our results by trajectories generated from Brownian dynamics simulations. Interestingly, transition path shapes are intrinsically asymmetric, they start out with finite slope and reach the target position with vanishing slope when plotted as mean time versus position, which is easily understood from one of our sum rules for transition path and passage times in Eq. (48).

The mean path shapes we predict can be compared straightforwardly with simulations of two state systems, for example, of proteins that undergo folding and unfolding events. This comparison will allow for a crucial test of the assumptions underlying the projection onto a one-dimensional reaction coordinate. With further developments of experimental single-molecule techniques, our results for the transition path shapes can also be compared with experimental results in the future. For such a comparison, note that a reflecting boundary condition at $x = x_A$, as used in our calculations, is typically neither present in molecular dynamics simulations nor in experiments. To apply our formulas, one would in practice shift the position of the reflecting boundary condition x_A to a position where the trajectory never visits.

ACKNOWLEDGMENTS

The authors thank Bill Eaton for stimulating discussions. Financial support from the DFG (Grant Nos. SFB 1078 and SFB 1114) is acknowledged.

[1]D. M. Zuckerman and T. B. Woolf, Phys. Rev. E **63**, 016702 (2000).
[2]P. G. Bolhuis, D. Chandler, C. Dellago, and P. L. Geissler, Annu. Rev. Phys. Chem. **53**, 291 (2002).
[3]R. B. Best and G. Hummer, Proc. Natl. Acad. Sci. U. S. A. **102**, 6732 (2005).
[4]P. Metzner, C. Schütte, and E. Vanden-Eijnden, J. Chem. Phys. **125**, 084110 (2006).
[5]G. Hummer, J. Chem. Phys. **120**, 516 (2004).
[6]H. S. Chung and I. V. Gopich, Phys. Chem. Chem. Phys. **16**, 18644 (2014).
[7]S. Chaudhury and D. E. Makarov, J. Chem. Phys. **133**, 034118 (2010).
[8]E. Rhoades, M. Cohen, B. Schuler, and G. Haran, J. Am. Chem. Soc. **126**, 14686 (2004).
[9]H. S. Chung, J. M. Louis, and W. A. Eaton, Proc. Natl. Acad. Sci. U. S. A. **106**, 11837 (2009).
[10]H. S. Chung, K. McHale, J. M. Louis, and W. A. Eaton, Science **335**, 981 (2012).
[11]H. S. Chung and W. A. Eaton, Nature **502**, 685 (2013).
[12]K. Neupane, D. B. Ritchie, H. Yu, D. A. N. Foster, F. Wang, and M. T. Woodside, Phys. Rev. Lett. **109**, 068102 (2012).
[13]K. Truex, H. S. Chung, J. M. Louis, and W. A. Eaton, Phys. Rev. Lett. **115**, 018101 (2015).
[14]H. Yu, A. N. Gupta, X. Liu, K. Neupane, A. M. Brigley, I. Sosova, and M. T. Woodside, Proc. Natl. Acad. Sci. U. S. A. **109**, 14452 (2012).
[15]I. V. Gopich and A. Szabo, J. Phys. Chem. B **113**, 10965 (2009).
[16]D. E. Shaw, P. Maragakis, K. Lindorff-Larsen, S. Piana, R. O. Dror, M. P. Eastwood, J. A. Bank, J. M. Jumper, J. K. Salmon, Y. Shan, and W. Wriggers, Science **330**, 341 (2010).
[17]Z. Zhang and H. S. Chan, Proc. Natl. Acad. Sci. U. S. A. **109**, 20919 (2012).
[18]R. Frederickx, T. in't Veld, and E. Carlon, Phys. Rev. Lett. **112**, 198102 (2014).
[19]B. W. Zhang, D. Jasnow, and D. M. Zuckerman, J. Chem. Phys. **126**, 074504 (2007).
[20]M. Sega, P. Faccioli, F. Pederiva, G. Garberoglio, and H. Orland, Phys. Rev. Lett. **99**, 118102 (2007).
[21]H. Orland, J. Chem. Phys. **134**, 174114 (2011).
[22]G. H. Weiss, Adv. Chem. Phys. **13**, 1 (1967).
[23]A. Szabo, K. Schulten, and Z. Schulten, J. Chem. Phys. **72**, 4350 (1980).
[24]R. Zwanzig, *Nonequilibrium Statistical Mechanics* (Oxford University Press, USA, 2001).
[25]M. Hinczewski, Y. von Hansen, J. Dzubiella, and R. R. Netz, J. Chem. Phys. **132**, 245103 (2010).
[26]Y. von Hansen, F. Sedlmeier, M. Hinczewski, and R. R. Netz, Phys. Rev. E **84**, 051501 (2011).
[27]D. R. Cox, *Renewal Theory* (Methuen, London, 1962), Vol. 4.
[28]N. G. Van Kampen, *Stochastic Processes in Physics and Chemistry* (Elsevier, 1992), Vol. 1.
[29]C. W. Gardiner, *Handbook of Stochastic Methods* (Springer, Berlin, 1985), Vol. 4.